Chemical Science

ROYAL SOCIETY OF CHEMISTRY

EDGE ARTICLE

View Article Online
View Journal | View Issue

Cite this: *Chem. Sci.*, 2023, **14**, 7185

All publication charges for this article have been paid for by the Royal Society of Chemistry

Received 22nd March 2023
Accepted 31st May 2023

DOI: 10.1039/d3sc01495a

rsc.li/chemical-science

Bidirectional photoswitchability in an iron(III) spin crossover complex: symmetry-breaking and solvent effects†

Raúl Díaz-Torres, ‡[a] Guillaume Chastanet, [b] Eric Collet, [c] Elzbieta Trzop, [c] Phimphaka Harding ‡*[d] and David J. Harding ‡*[d]

The impact of solvent on spin crossover (SCO) behaviour is reported in two solvates $[Fe(qsal\text{-}I)_2]NO_3\cdot 2ROH$ (qsal-I = 4-iodo-2-[(8-quinolylimino)methyl]phenolate; R = Me **1** or Et **2**) which undergo abrupt and gradual SCO, respectively. A symmetry-breaking phase transition due to spin-state ordering from a [HS] to [HS-LS] state occurs at 210 K in **1**, while $T_{1/2}$ = 250 K for the EtOH solvate, where complete SCO occurs. The MeOH solvate exhibits LIESST and *reverse*-LIESST from the [HS-LS] state, revealing a hidden [LS] state. Moreover, photocrystallographic studies on **1** at 10 K reveal re-entrant photoinduced phase transitions to a high symmetry [HS] phase when irradiated at 980 nm or a high symmetry [LS] phase after irradiation at 660 nm. This study represents the first example of bidirectional photoswitchability and subsequent symmetry-breaking from a [HS-LS] state in an iron(III) SCO material.

Introduction

The search for bistable molecular systems is driven by their possible applications in molecular electronic devices.[1,2] Spin crossover (SCO) complexes are one group of bistable materials that have been utilised as functional components in a range of devices.[3–5] The interest lies in the appreciable changes in the magnetic and physical properties upon transition between the low spin (LS) and high spin (HS) state, induced by an external perturbation (temperature, pressure, light irradiation or magnetic field). In the majority of SCO complexes, these changes are gradual making them less attractive for applications. However, SCO complexes with abrupt transitions result in dramatic changes in their properties, and are excellent prototypes for use in molecular sensors, switches, data storage or spintronics.[6,7] To achieve abrupt SCO, strong interactions between the SCO centres, the so-called cooperativity, are required with two different strategies employed: the polymeric approach, where covalent bonds are used to directly connect the spin sites,[8,9] and the supramolecular approach, where intermolecular interactions are employed (π–π, hydrogen and halogen bonds), which have the advantage of being more elastic.[10–12] These interactions are responsible for transmitting structural distortions along the crystal as the spin transition occurs. In most cases, this results in a single-step spin transition, sometimes with hysteresis. However, multi-step transitions can also occur[13,14] often due to the presence of inequivalent spin centres that undergo SCO at different temperatures. More rarely, previously equivalent sites become inequivalent upon SCO in a process termed symmetry-breaking (SB).[15–19] The first example of SB in Fe^{III} was reported by Morgan and co-workers[20] in $[Fe^{III}(3,5\text{-OMe-sal}_2bapen)]ClO_4$ {3,5-OMe-sal_2bapen = *N*,*N*′-bis(3,5-dimethoxysalicylidene)-1,5,8,12-tetraazadodecane} where incomplete SCO occurs in three steps from HS → [2HS-LS] → [HS-2LS]. Since then a number of SB SCO systems have been discovered with $[Fe^{III}(H\text{-}5\text{-}Br\text{-}thsa)(5\text{-}Br\text{-}thsa)]\cdot H_2O$ (H_2-5-Br-thsa = 5-bromo-2-hydroxy(benzylidene) hydrazinecarbothioamide) exhibiting a remarkable 5-step SCO.[21]

Quinolylsalicylaldiminate complexes are particularly prevalent in iron(III) SCO chemistry[22–25] with three SB examples now known. $[Fe(qsal\text{-}Br)_2]NO_3\cdot 2MeOH$ (qsal-Br = 4-bromo-2-[(8-quinolylimino)methyl]phenolate),[26] exhibits SB coupled to a complete two-step SCO through HS (1 centre) → [HS-LS] (2 centres) → LS (1 centre), showing an intermediate phase (IP) [HS-LS] plateau of 96 K. $[Fe(qsal)_2][(C_6F_3I_3)I]$ also shows SB from HS (1 centre) → [HS-LS] (2 centres), with the LS state thermally inaccessible.[27] Lastly,

[a]*Thammasat University Research Unit in Multifunctional Crystalline Materials and Applications (TU-MCMA), Faculty of Science and Technology, Thammasat University, Pathum Thani 12121, Thailand*

[b]*Université de Bordeaux, ICMCB, 87 Avenue du Dr A. Schweitzer, Pessac, F-33608, France*

[c]*Univ Rennes, CNRS, IPR (Institut de Physique de Rennes) – UMR 6251, F-35000 Rennes, France*

[d]*School of Chemistry, Institute of Science, Suranaree University of Technology, Nakhon Ratchasima, 30000, Thailand. E-mail: david@g.sut.ac.th; phimphaka@g.sut.ac.th*

† Electronic supplementary information (ESI) available: Experimental details, X-ray crystallographic data, additional structural, magnetic and TGA figures. CCDC 2220036–2220047. For ESI and crystallographic data in CIF or other electronic format see DOI: https://doi.org/10.1039/d3sc01495a

‡ Previous address: Functional Materials and Nanotechnology Centre of Excellence, Walailak University, Thasala, Nakhon Si Thammarat, 80160, Thailand

$[Fe(qsal\text{-}4\text{-}F)_2]NO_3 \cdot 0.91MeOH \cdot 0.57H_2O$ (qsal-4-F = 5-fluoro-2-[(8-quinolylimino)methyl]phenolate) exhibits SCO in two steps, but this time from HS → [HS-LS] → [LS-LS], with no re-entrant LS phase.[28] Recent studies suggest that symmetry-breaking and SCO phenomena are coupled through volume strain.[29,30] This behaviour emerges through the appearance of competing short/long range elastic interactions (*e.g.* H-bonds, π–π interactions) in the crystal.[31] In molecular systems, symmetry-breaking most often occurs when previously equivalent sites become ordered into patterns of HS and LS states driven in part by these elastic interactions. However, a lack of systematic studies, especially for Fe^{III}, that probe the influence of each factor on symmetry-breaking has made it difficult to improve these systems.

Light-Induced Excited Spin-State Trapping or LIESST involves light activation of a SCO material, typically from a LS to a HS state. The vast majority of reports concern Fe^{II} complexes,[32–36] with comparatively few known for Fe^{III}.[37–39] The first Fe^{III} complex known to exhibit LIESST was $[Fe(pap)_2]ClO_4 \cdot H_2O$ (pap = 2-[(pyrid-2-yl)methyleneamino]phenolate) reported by Sato and co-workers[40] in 2000. Subsequent work seems to indicate that large distortions at the metal centre are key to the observation of LIESST in Fe^{III} systems.[41] Interestingly, for both Fe^{II} and Fe^{III} it is also possible to use a different wavelength of light to switch from the metastable HS state back to the LS state, a process known as *reverse*-LIESST (Fig. 1a). Moreover, light irradiation sometimes permits access to hidden spin states that are not accessible thermally (Fig. 1b). While common in coordination polymers,[42–47] we are aware of only one mononuclear complex where this has been observed.[38] In this work we present a study of $[Fe(qsal\text{-}I)_2]NO_3 \cdot 2ROH$ (qsal-I = 4-iodo-2-[(8-quinolylimino)methyl]phenolate; R = Me **1**, Et **2**) where the different alcohols result in symmetry-breaking SCO or non-symmetry breaking and gradual SCO, respectively and compare it with bromo- analog $[Fe(qsal\text{-}Br)_2]NO_3 \cdot 2MeOH$ (**3**).[26] Remarkably, **1** exhibits bidirectional switching from the low symmetry [HS-LS] state, allowing access to a hidden LS state or a HS state, both of higher symmetry.

Results and discussion

Synthesis

Both compounds were prepared by layering a solution of $Fe(NO_3)_3 \cdot 9H_2O$ in MeOH (**1**) or EtOH (**2**) over a solution of Hqsal-I in CH_2Cl_2 in which NEt_3 had been added. Full spectroscopic and Experimental details can be found in the ESI† and are consistent with the proposed formulae.

Structural descriptions

The crystal structure of **2** was collected at 300 and 150 K with the asymmetric unit showing one $[Fe(qsal\text{-}I)_2]^+$ cation, a nitrate anion and two ethanol molecules at both temperatures (Fig. S1†). For **1**, symmetry-breaking is observed, showing one independent Fe^{III} centre at high temperature (300, 240 K), and two centres (Fe1 and Fe2) at low temperature (150 and 100 K; Table S1†). Both compounds crystallize in triclinic $P\bar{1}$ with a *pseudo*-octahedral Fe^{III} metal centre and two meridionally coordinated qsal-I ligands (Fig. 2). In **1**, the Fe-N_{av} distances and octahedral distortion parameters[48] indicate HS Fe^{III} at 300 K (*ca.* d_{av}Fe1–N = 2.132 Å and Θ = 235, respectively),[49] while at 240 K they shrink slightly to *ca.* d_{av}Fe1 = 2.082 Å and Θ = 187, consistent with *ca.* 80% HS. Further cooling to 150 K results in doubling of the unit cell volume ($V_{300\ K}$ = 1699 $Å^3$; $V_{150\ K}$ = 3316 $Å^3$), indicating symmetry-breaking and resulting in two $[Fe(qsal\text{-}I)_2]^+$ cations in the doubled asymmetric unit (Fig. 1). At this temperature, the Fe-N_{av} distances are Fe1–N = 1.96 Å and Fe2–N = 2.13 Å respectively, showing that Fe1 is LS while Fe2 is HS.[49] This long-range ordering of HS and LS molecular states corresponds to the formation of a spin-state concentration wave, SSCW.[29] No significant changes are observed between 150 K and 100 K (Table S2†).

Heating back to 300 K, reveals reversible spin conversion and an increase in symmetry with a single Fe^{III} centre in the asymmetric unit. The reversibility of symmetry-breaking SCO was confirmed by recooling to 150 K with the structure again showing two independent Fe^{III} centres. This behaviour is similar to $[Fe(qsal\text{-}Br)_2]NO_3 \cdot 2MeOH$ **3**,[26] but the iodo group seems to prevent access to the full LS state, presumably because of its steric bulk that favours stronger antiferroelastic interactions between the Fe^{III} centres stabilizing [HS-LS] order.[22] There are comparatively few Fe^{III} systems that undergo symmetry-breaking SCO[18,20,50–53] and this is only the third example from a [HS] to an ordered [HS-LS] SSCW (Table S3†).[54]

The ethanol complex, **2** has simpler behaviour, with Fe–N/O distances (Fe-N_{av} = 2.12, Fe-O_{av} = 1.90 Å) and octahedral

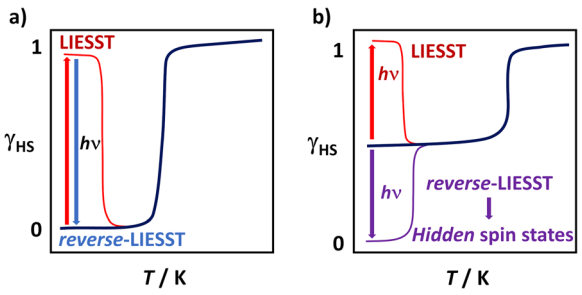

Fig. 1 Visual representation of (a) LIESST and *reverse*-LIESST and (b) light activation to access hidden (not easily accessible) spin states.

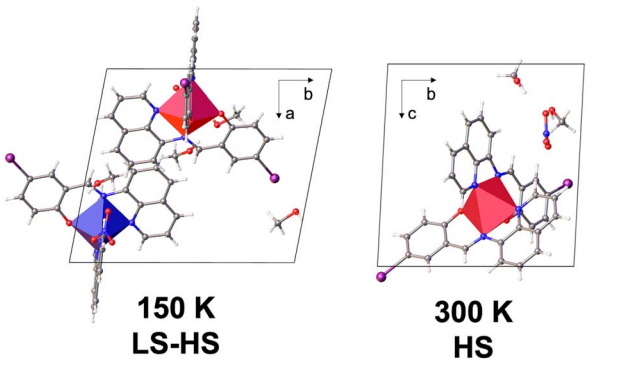

Fig. 2 Unit cell components of **1** at 150 K (left) and 300 K (right). The *a*, *b* and *c* axis at 300 K and 150 K correspond to different directions.

parameters ($\Sigma = 59$ and $\Theta = 204$) at 300 K consistent with HS Fe^{III}.[49] Cooling to 150 K, results in a decrease in the Fe–N/O bond distances (ΔFe-$N_{av} = 0.137$ and ΔFe-$O_{av} = 0.025$) and the octahedral parameters ($\Delta\Sigma = 15$ and $\Delta\Theta = 87$) indicating a HS to LS transition (Table S4†). The lack of symmetry-breaking in **2** suggests that the methanol solvent is primarily responsible, modifying elastic interactions between the Fe^{III} centres, mirroring results reported for $[Fe(1\text{-bpp-SiPr})_2][BF_4]_2\cdot$sol (1-bpp-SiPr = 1-bpp-SiPr = 2,6-di{pyrazol-1-yl}-4-isopropylthiopyridine).[55]

Crystal packing

The packing in the structures consist of 1D chains along the *c* axis (Fig. 3 and S2†) where the Fe^{III} cations are connected *via* two sets of perpendicular π–π interactions (Type A and Type B) supported by C–H···O interactions. In the case of **1** at 150 K, symmetry-breaking does not alter the packing of the Fe^{III} cations with each Fe centre in separate 1D chains (Fe1–Fe1 and Fe2–Fe2) as shown in Fig. 3. The π–π distances in **1** and **2** are similar, with Type B being slightly stronger (by about 0.12 Å) compared to Type A. One of the most significant differences between **1** and **2** is the shorter Fe–Fe distance within the 1D chain for **1**, by about 0.3 Å. This feature is also observed in the P4AE (parallel fourfold aryl embraces)[56] and C–H···I interactions, that connect neighbouring 1D chains and form a 2D sheet in the (*ac*) plane (Fig. 3 and S3†). In both cases, the interactions are much shorter for **1** (by about 0.3 Å) compared to **2**. The final 3D structure is formed by C–H···I interactions connecting the 2D planes along the *b* axis (Fig. 3). This higher dimensional structure is also supported by halogen bonds (I···I) in the case of **1** (Fig. S4 and S5†).

The nitrate and solvent molecules (MeOH for **1** and EtOH for **2**) are mainly located in the space between the chains (Fig. S6†). These molecules interact by C–H···O, O–H···O and O···I contacts and aid in the formation of the 2D structure by connecting the qsal-I ligands from different chains. This results in the formation of a supramolecular square (Fig. S6†). In the case of **2**, the halogen bond (N–O···I) is slightly stronger (3.37 Å) than in **1** (3.51 Å). In all cases, small changes are observed with temperature.

The distance between the chains (termed d_{chain}) is affected by the solvent's size, being shorter for **1** and **3** (12.0 Å) compared to **2** (12.3 Å) at 300 K and consistent with the more compact structure for **1** (Fig. 4, S7 and Table S5†). In the case of **2**, d_{chain} does not show any variation with temperature, while for **1** and **3**, after symmetry breaking, the distances become longer and shorter by *ca.* 0.25 Å for Fe1 HS and Fe2 LS chains, respectively. Interestingly, in **3**, d_{chain} in the LS state is slightly higher than that in the HS state. In contrast, the distance between the planes (termed d_{plane}) is slightly higher for **1**, 12.5 Å, compared to 12.3 Å for **2** and **3**. The similarity in d_{plane} in **2** and **3** is unexpected but may be *a* factor in the thermal inaccessibility of the LS state in **1**, as the iodo substituents are located between the planes. Overall, the shorter Fe–Fe distances *within* the chains and the lower d_{chain} values that reflect the distance *between* the chains indicate that the more compact structure in **1** enhances elastic interactions between the Fe^{III} centres and the antiferroelastic interactions that favour [HS-LS] ordering and long-range ordered SSCW.[29,30,57]

To better quantify the supramolecular interactions present in **1–3** we undertook Hirshfeld analysis. This reveals no significant differences between the compounds. The contributions, as well as their strength, are broadly similar in all systems

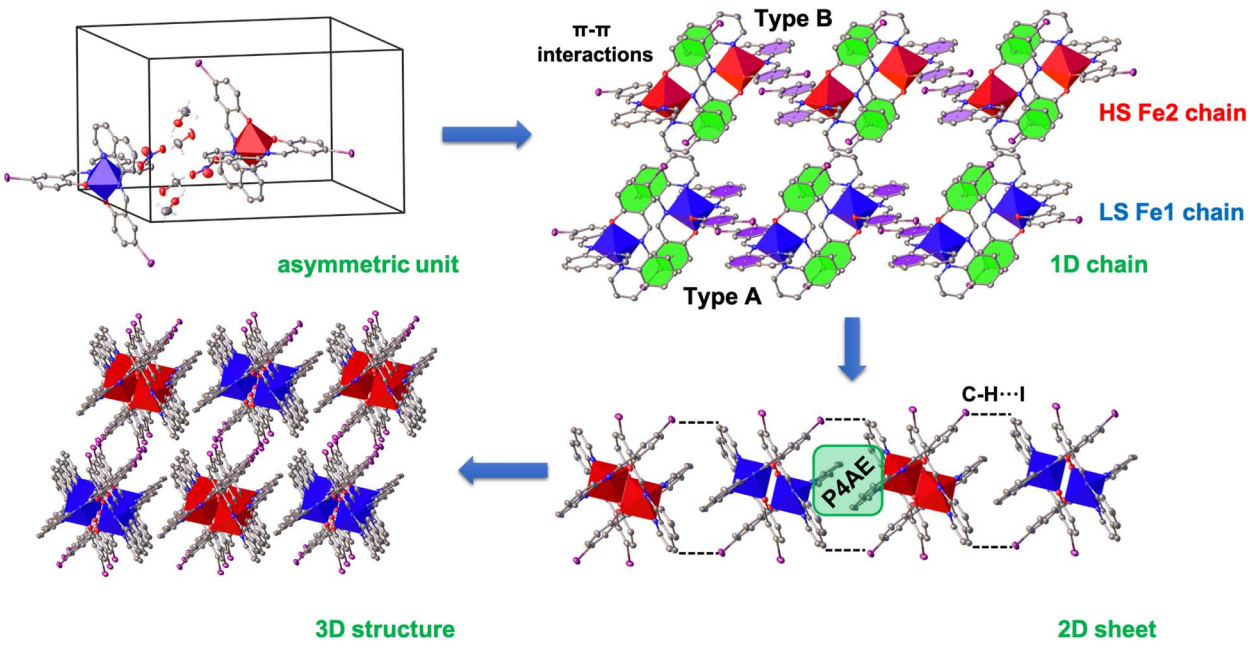

Fig. 3 Schematic illustration of the packing from the asymmetric unit to the final supramolecular 3D structure for **1** at 150 K (blue Fe1 centres, red Fe2 centres). This figure is intended as a guide to the discussion only.

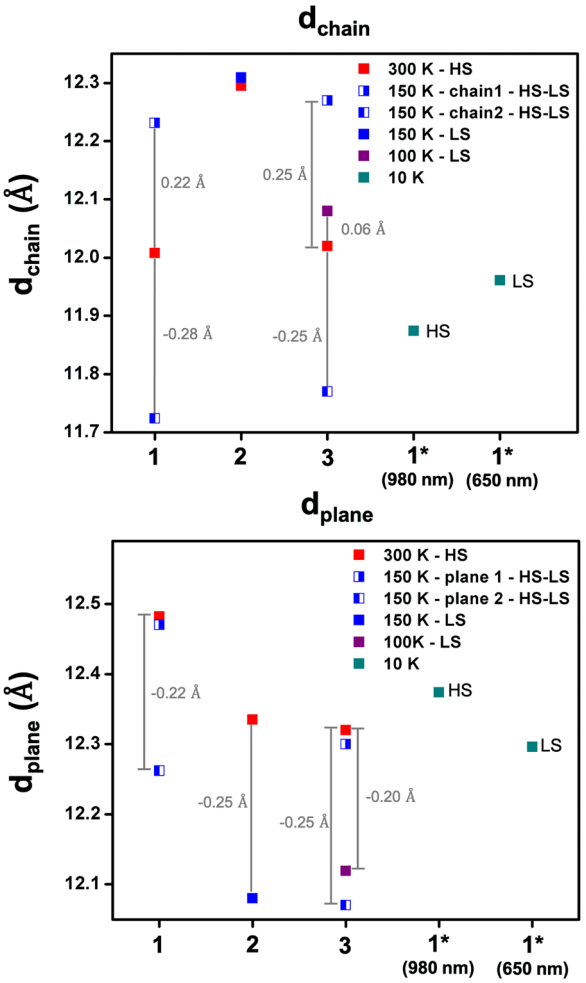

Fig. 4 Plots of the variation of the d_{chain} (top) and d_{plane} (bottom) for **1**, **2**, and **3** at different temperatures. The changes in these values are indicated by the grey bars. *indicates irradiated samples.

(Table S8, Fig. S8 and S9†). The one exception is the O···H/H···O interactions, which are significantly stronger for the MeOH complexes (1.7 and 2.0 Å, for **1** and **3**, respectively) compared to **2** (2.5 Å) at 300 K. The reason for this difference is that in **2** at 300 K one of the ethanol molecules is disordered. However, upon cooling, the hydrogen bonds in **2** become much stronger (2.05 Å), whereas for **1** weaker hydrogen bonding is observed (2.25 Å). The fact that this change is not observed in **3**, where the values remain almost unchanged, strongly suggests that the SB process is unlikely to be related to these changes in the hydrogen bonding contacts.

Magnetic studies

Magnetic susceptibility data recorded on polycrystalline samples of **1** and **2** between 5–300 K, are shown in Fig. 5 and S10–S13.† At 300 K, the $\chi_M T$ values for **1** and **2** are *ca.* 3.90–4.10 cm^3 K mol^{-1} consistent with the HS state.[49] Cooling of **1** shows a moderately abrupt SCO (ΔT_{80} = 70 K; defined as the temperature range over which the SCO is 80% complete)[58] with $T_{1/2}$ = 210 K. At 150 K, $\chi_M T$ = 2.40 cm^3 K mol^{-1} and consistent with the [HS-LS] state observed crystallographically. Interestingly, a further decrease in $\chi_M T$ is observed around 80 K reaching a value of 2.15 cm^3 K mol^{-1}. It is important to note that this behaviour is repeatable over several measurements and the additional step at 80 K does not depend on kinetics (see Fig. S10†). Moreover, a structure collected at 10 K shows no changes in the Fe–N/O bond lengths despite this small decrease in $\chi_M T$ (Table S2†). For **2**, cooling results in a more gradual change (ΔT_{80} = 88 K) in $\chi_M T$, reaching a value of 0.60 cm^3 K mol^{-1} at 150 K, indicative of the full LS state (Fig. 5 and S11†). In this case $T_{1/2}$ is around 250 K, 40 K higher than in **1** suggesting that the slight differences in the packing in the EtOH solvate modifies the ligand field thereby favouring the LS state in **2**. At high temperatures, the SCO profiles change markedly due to desolvation (Fig. S12–S14†), in agreement with TGA analysis (Fig. S15†). After heating to 350 K, both samples exhibit slightly different profiles (Fig. S14†), probably due to differing degrees of incomplete desolvation. However, in both cases a much more gradual SCO (ΔT_{80} = 178 K) than either of the solvates are observed. The trapping of **1** in the [HS-LS] state contrasts with $[Fe(qsal\text{-}Br)_2]NO_3 \cdot 2MeOH$ where the full LS state is accessible.[26] It would appear that the small increase in the van der Waal radius between the bromo (1.86 Å) and iodo atoms (2.04 Å) is sufficient to make the LS state thermally inaccessible.[59]

Photomagnetic studies

Photomagnetic studies on **1** reveal that at 10 K irradiation at 980 nm causes an increase in $\chi_M T$ reaching 3.38 cm^3 K mol^{-1} at 20 K and indicative of LIESST. The photoconversion efficiency is *ca.* 67% and one of the most efficient yet reported for Fe^{III} (Table S6 in the ESI†). The derivative of $\chi_M T$ *vs.* T reveals that T(LIESST) is 38 K. Interestingly, above 60 K the $\chi_M T$ values dip below the thermal SCO profile with an additional decrease of $\chi_M T$ at the same temperature then a small jump in the SCO curve. The reason for this remains unclear, but similar observations have

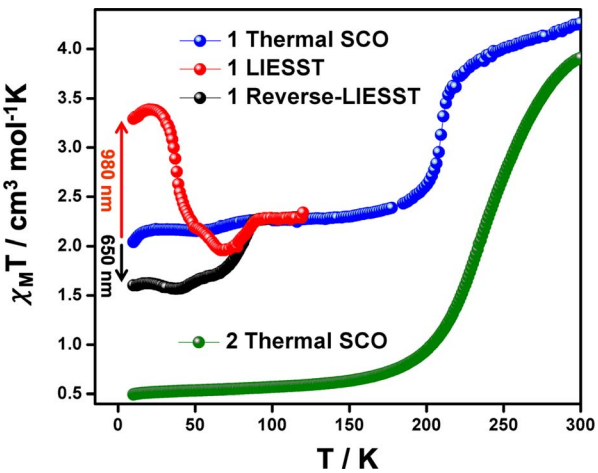

Fig. 5 $\chi_M T$ *versus* T plot (recorded at 0.5 K min^{-1}) of **1** showing the thermal behaviour in the dark without any previous light irradiation (blue), after LIESST effect at 980 nm (red) and after *reverse*-LIESST effect at 650 nm (black) and thermal behaviour of **2** (green).

been noted in $[Fe(qsal)_2][(C_6F_3I_3)I]$.[27] One possible explanation is that relaxation from the high-symmetry HS state proceeds initially to a metastable LS state of the same symmetry, before further warming results in SB to the long-range ordered [HS-LS] SSCW state. No LIESST effect was observed in **2**, mirroring the results found in **3**. Given how similar the supramolecular contacts are in **1** and **2** (see Hirshfeld analysis above) it seems likely that the SB that occurs in **1**, but not in **2** is responsible. Symmetry-breaking is also not required in **3** as the LS state is of high symmetry and may explain the lack of LIESST in this system. This is consistent with the surprisingly different T(LIESST) values in the MeCN and $MeNO_2$ solvates of $[Fe(1\text{-bpp-SiPr})_2][BF_4]_2\cdot$sol.[55] The MeCN solvate shows no SB and is observed on the normal T(LIESST) line for this class of compound. In contrast, the $MeNO_2$ solvate exhibits SB from a LS ($P2_1/c$, $Z = 12$) phase to a HS ($P2_1$, $Z = 4$) phase, upon light irradiation, and a lower than expected T(LIESST) value. In the case of Fe^{III}, where relaxation is generally more rapid,[37,60] perhaps SB permits observation of LIESST in compounds where it is not normally observed. The presence of efficient LIESST in $[Fe^{III}(psalpm\text{-}Cl)_2]$PTFB (psalpm-Cl = 4-chloro-(*R*,*S*)-((phenyl(2-pyridyl)methylimino)methyl)phenolate; PTFB = phenyltrifluoroborate)[54] and $[Fe(qsal)_2][(C_6F_3I_3)I]$.[27] would seem to support this hypothesis. However, no structural data is available for either compound in the photoinduced HS state and further examples will be needed to see if this is a more general trend. Overall, these observations support the fact that the lifetime of the photo-induced state does not depend exclusively on the coordination sphere parameters but is also influenced by all the additional energies associated with symmetry changes, such as SB and order-disorder transitions.

The strong *reverse*-LIESST exhibited by $[Fe(naphBzen)_2]I$[38] encouraged us to irradiate **1** with 650 nm light. While the *reverse*-LIESST is far from complete, there is a clear drop in $\chi_M T$, which reaches 1.60 cm^3 K mol^{-1} at 10 K. This value is maintained until 45 K, after which it increases gradually, before a more rapid rise to rejoin the thermal SCO profile at 90 K. The presence of significant LIESST and *reverse*-LIESST from a [HS-LS] state, formed upon symmetry-breaking, is to the best of our knowledge unique in Fe^{III} SCO chemistry. Interestingly, $[Fe(qsal)_2][(C_6F_3I_3)I]$ when irradiated at 650 nm shows relaxation from the meta-stable HS state to the [HS-LS] state with no evidence of a hidden LS state.[27] Moreover, it appears that the multistep character of the thermal SCO is maintained in the curves recorded after LIESST and *reverse*-LIESST effects.

Photocrystallographic studies

Photocrystallographic studies were conducted on **1** at 10 K by irradiating a crystal at 980 and 660 nm. In both cases, the structures retain triclinic symmetry but now contain a single Fe^{III} centre with the same lattice periodicity as the high temperature HS phase, as the initially different [HS-LS] sites become equivalent in the fully [HS] or [LS] states. It is likely that this high symmetry recovery, which corresponds to a photoinduced re-entrant phenomena, is responsible for the relatively strong LIESST and *reverse*-LIESST that is observed in **1**,[55] due to the elastic coupling between the spin state and symmetry changes.[29] In the 980 nm structure, the bond lengths are indicative of HS Fe^{III}, while the Fe-N_{ave} distances in the 660 nm structure are 1.98 Å and typical for LS Fe^{III}, Fig. 6. This is supported by the octahedral distortion parameters which are $\Sigma = 61$ and $\Theta = 228$ (HS-980 nm) and $\Sigma = 41$ and $\Theta = 118$ (LS-660 nm). We note that d_{chain} and d_{plane} in the photoinduced HS and LS structures show relatively small changes upon SCO by 0.09 and 0.08 Å, respectively (Table S5† and Fig. 4). As observed in **3**, d_{chain} is shorter in the HS structure, while d_{plane} is shorter in the LS structure. However, **3** (HS and LS structures only) shows a smaller change in d_{chain} (0.06 Å), but a much larger change in d_{plane} (0.21 Å). The complete SCO observed in the single crystal contrasts with the incomplete LIESST and *reverse*-LIESST observed in the magnetic studies and probably reflects the extremely dark colour of the crystals which limits light penetration in the bulk.[34,61,62] The HS structure at 300 K and that of the photoinduced HS structure at 10 K are almost identical. Moreover, the packing in the photoinduced HS and LS structures closely mirrors that at 300 K but with much shorter supramolecular contacts (see ESI Table S7†). An interesting difference is that the O(nitrate)···I halogen bond is lost in the LS structure (Fig. S16†).

Comparing **1** with existing SCO systems it is important to note that the thermal SCO and SB are clearly coupled. This is not the case in previously studied examples where a 'hidden' LS state is present.[38,43,63] Hence, in **1** at 10 K where there are two distinct Fe^{III} centres, one HS and the other LS, a change in both symmetry (2 Fe^{III} centres to 1 Fe^{III} centre) and spin state is required to access the LS state. In this case the phase transition is reconstructive as the fully LS phase is of higher symmetry than the [HS-LS] phase and therefore the phase transition is discontinuous and associated with latent heat. Recalling that the low symmetry [HS-LS] state is stabilized through the elastic coupling of the SB to the volume strain,[29] there is an elastic cost to reach the high symmetry fully LS state, which makes it

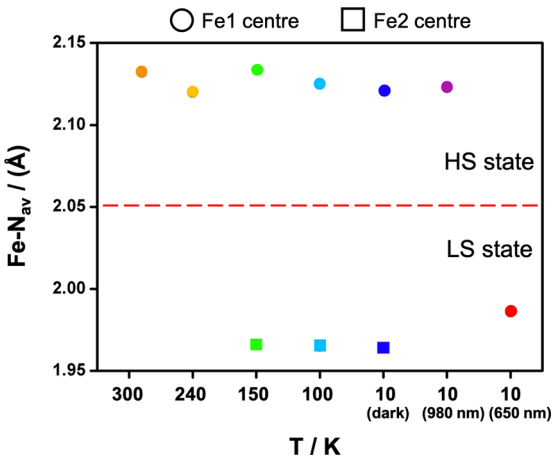

Fig. 6 Plot of the Fe-N_{av} distance for **1** at 300 K (orange), 240 K (yellow), 150 K (green), 100 K (light blue), 10 K (blue), 10 K (980 nm) (purple) and 10 K (660 nm) (red). Circles represent the Fe1 centre and squares the Fe2 centre.

inaccessible at low temperature following a thermal equilibrium path. However, in the case of relaxation from the LIESST HS state, a relaxation towards the fully LS state is made easier because there is no symmetry change between these states, and therefore no elastic cost related to symmetry-breaking.

Conclusions

In summary, we have explored the impact of two alcohol solvents on SCO behaviour in an Fe^{III} SCO complex. While the EtOH solvate exhibits a gradual, complete and single step SCO, the MeOH solvate shows a rare symmetry-breaking spin transition to a long-range ordered [HS-LS] SSCW state combined with a re-entrant photoinduced phase transition towards HS or hidden LS states under irradiation with visible or near-IR light. The results demonstrate how solvent subtly alters the packing in the structure, allowing for chemical tuning of the supramolecular interactions between the active SCO centres and favouring here incomplete symmetry-breaking SCO in **1**, which in turn permits bidirectional switching in an Fe^{III} SCO material. Moreover, the results suggest that SB seems to favour LIESST in Fe^{III}, although further structural studies will be needed to determine how applicable the observations in **1** are to other Fe^{III} complexes.

Data availability

Magnetic data for this article are available upon request.

Author contributions

Raúl Díaz-Torres: investigation, formal analysis, data curation, visualization, writing – original draft. Guillaume Chastanet: investigation, formal analysis, data curation, writing – review & editing. Eric Collet: investigation, data curation, writing – review & editing. Elzbieta Trzop: methodology, investigation, formal analysis, data curation. Phimphaka Harding: conceptualization, resources, writing – review & editing, supervision. David J. Harding: conceptualization, resources, writing – review & editing, supervision, funding acquisition.

Conflicts of interest

There are no conflicts to declare.

Acknowledgements

We gratefully acknowledge the National Research Council of Thailand (NRCT) grant number NRCT5-RSA63019-02 for funding. Walailak University is thanked for a postdoctoral research fellowship to R. D. T. The National Science Technology and Innovation Policy Office for Integrated Research and Innovation Plan (Grant No. 256113A3050001) is thanked for funds to purchase an X-ray diffractometer.

Notes and references

1 M. Ratner, *Nat. Nanotechnol.*, 2013, **8**, 378–381.
2 H. Song, M. A. Reed and T. Lee, *Adv. Mater.*, 2011, **23**, 1583–1608.
3 G. Molnár, S. Rat, L. Salmon, W. Nicolazzi and A. Bousseksou, *Adv. Mater.*, 2018, **30**, 1–23.
4 J.-F. Létard, P. Guionneau and L. Goux-Capes, in *Spin Crossover in Transition Metal Compounds III*, Springer-Verlag, Berlin/Heidelberg, 2004, pp. 221–249.
5 K. Senthil Kumar and M. Ruben, *Coord. Chem. Rev.*, 2017, **346**, 176–205.
6 Z.-P. Ni, J.-L. Liu, M. N. Hoque, W. Liu, J.-Y. Li, Y.-C. Chen and M.-L. Tong, *Coord. Chem. Rev.*, 2017, **335**, 28–43.
7 J. Linares, E. Codjovi and Y. Garcia, *Sensors*, 2012, **12**, 4479–4492.
8 K. A. Zenere, S. G. Duyker, E. Trzop, E. Collet, B. Chan, P. W. Doheny, C. J. Kepert and S. M. Neville, *Chem. Sci.*, 2018, **9**, 5623–5629.
9 D. J. Mondal, S. Roy, J. Yadav, M. Zeller and S. Konar, *Inorg. Chem.*, 2020, **59**, 13024–13028.
10 W. Phonsri, D. J. Harding, P. Harding, K. S. Murray, B. Moubaraki, I. A. Gass, J. D. Cashion, G. N. L. Jameson and H. Adams, *Dalton Trans.*, 2014, **43**, 17509–17518.
11 A. Tsukiashi, M. Nakaya, F. Kobayashi, R. Ohtani, M. Nakamura, J. M. Harrowfield, Y. Kim and S. Hayami, *Inorg. Chem.*, 2018, **57**, 2834–2842.
12 G. Dupouy, M. Marchivie, S. Triki, J. Sala-Pala, J.-Y. Salaün, C. J. Gómez-García and P. Guionneau, *Inorg. Chem.*, 2008, **47**, 8921–8931.
13 Y. Y. Peng, S. G. Wu, Y. C. Chen, W. Liu, G. Z. Huang, Z. P. Ni and M. L. Tong, *Inorg. Chem. Front.*, 2020, **7**, 1685–1690.
14 F. Fürmeyer, L. M. Carrella, V. Ksenofontov, A. Möller and E. Rentschler, *Inorg. Chem.*, 2020, **59**, 2843–2852.
15 M. Shatruk, H. Phan, B. A. Chrisostomo and A. Suleimenova, *Coord. Chem. Rev.*, 2015, **289–290**, 62–73.
16 C. Zheng, S. Jia, Y. Dong, J. Xu, H. Sui, F. Wang and D. Li, *Inorg. Chem.*, 2019, **58**, 14316–14324.
17 Y. Meng, Q. Q. Sheng, M. N. Hoque, Y. C. Chen, S. G. Wu, J. Tucek, R. Zboril, T. Liu, Z. P. Ni and M. L. Tong, *Chem.–Eur. J.*, 2017, **23**, 10034–10037.
18 Z. Y. Li, J. W. Dai, Y. Shiota, K. Yoshizawa, S. Kanegawa and O. Sato, *Chem.–Eur. J.*, 2013, **19**, 12948–12952.
19 E. Trzop, D. Zhang, L. Piñeiro-Lopez, F. J. Valverde-Muñoz, M. Carmen Muñoz, L. Palatinus, L. Guerin, H. Cailleau, J. A. Real and E. Collet, *Angew. Chem., Int. Ed.*, 2016, **55**, 8675–8679.
20 M. Griffin, S. Shakespeare, H. J. Shepherd, C. J. Harding, J. F. Létard, C. Desplanches, A. E. Goeta, J. A. K. Howard, A. K. Powell, V. Mereacre, Y. Garcia, A. D. Naik, H. Müller-Bunz and G. G. Morgan, *Angew. Chem., Int. Ed.*, 2011, **50**, 896–900.
21 Z.-Y. Li, H. Ohtsu, T. Kojima, J.-W. Dai, T. Yoshida, B. K. Breedlove, W.-X. Zhang, H. Iguchi, O. Sato, M. Kawano and M. Yamashita, *Angew. Chem., Int. Ed.*, 2016, **55**, 5184–5189.
22 K. Takahashi, K. Yamamoto, T. Yamamoto, Y. Einaga, Y. Shiota, K. Yoshizawa and H. Mori, *Crystals*, 2019, **9**, 81.
23 B. J. C. Vieira, J. C. Dias, I. C. Santos, L. C. J. Pereira, V. da Gama and J. C. Waerenborgh, *Inorg. Chem.*, 2015, **54**, 1354–1362.

24 S. Hayami, Z. Z. Gu, H. Yoshiki, A. Fujishima and O. Sato, *J. Am. Chem. Soc.*, 2001, **123**, 11644–11650.
25 B. J. C. Vieira, L. C. J. Pereira, V. da Gama, I. C. Santos, A. C. Cerdeira and J. C. Waerenborgh, *Magnetochemistry*, 2021, **8**, 1.
26 D. J. Harding, W. Phonsri, P. Harding, K. S. Murray, B. Moubaraki and G. N. L. Jameson, *Dalton Trans.*, 2015, **44**, 15079–15082.
27 I. R. Jeon, C. Mathonière, R. Clérac, M. Rouzières, O. Jeannin, E. Trzop, E. Collet and M. Fourmigué, *Chem. Commun.*, 2017, **53**, 10283–10286.
28 H. J. Sheng, C. C. Xia, X. Y. Zhang, C. C. Zhang, W. J. Ji, Y. Zhao and X. Y. Wang, *Inorg. Chem.*, 2022, **61**, 12726–12735.
29 G. Azzolina, R. Bertoni and E. Collet, *J. Appl. Phys.*, 2021, **129**, 085106.
30 E. Collet and G. Azzolina, *Phys. Rev. Mater.*, 2021, **5**, 1–11.
31 N. Ortega-Villar, M. Muñoz and J. Real, *Magnetochemistry*, 2016, **2**, 16.
32 A. Hauser, *Top. Curr. Chem.*, 2012, **234**, 155–198.
33 M. A. Halcrow, *Chem. Soc. Rev.*, 2011, **40**, 4119–4142.
34 G. Chastanet, M. Lorenc, R. Bertoni and C. Desplanches, *C. R. Chim.*, 2018, **21**, 1075–1094.
35 T. T. Ma, X. P. Sun, Z. S. Yao and J. Tao, *Inorg. Chem. Front.*, 2020, **7**, 1196–1204.
36 V. García-López, M. Palacios-Corella, S. Cardona-Serra, M. Clemente-León and E. Coronado, *Chem. Commun.*, 2019, **55**, 12227–12230.
37 M. Nakaya, R. Ohtani, L. F. Lindoy and S. Hayami, *Inorg. Chem. Front.*, 2021, **8**, 484–498.
38 T. Boonprab, S. J. Lee, S. G. Telfer, K. S. Murray, W. Phonsri, G. Chastanet, E. Collet, E. Trzop, G. N. L. Jameson, P. Harding and D. J. Harding, *Angew. Chem., Int. Ed.*, 2019, **58**, 11811–11815.
39 M. Nakaya, K. Shimayama, K. Takami, K. Hirata, A. S. Alao, M. Nakamura, L. F. Lindoy and S. Hayami, *Chem. Lett.*, 2014, **43**, 1058–1060.
40 S. Hayami, Z. Gu, M. Shiro, Y. Einaga, A. Fujishima and O. Sato, *J. Am. Chem. Soc.*, 2000, **122**, 7126–7127.
41 S. Hayami, K. Hiki, T. Kawahara, Y. Maeda, D. Urakami, K. Inoue, M. Ohama, S. Kawata and O. Sato, *Chem.–Eur. J.*, 2009, **15**, 3497–3508.
42 H. Fourati, M. Ndiaye, M. Sy, S. Triki, G. Chastanet, S. Pillet and K. Boukheddaden, *Phys. Rev. B*, 2022, **105**, 174436.
43 K.-P. Xie, Z.-Y. Ruan, X.-X. Chen, J. Yang, S.-G. Wu, Z.-P. Ni and M.-L. Tong, *Inorg. Chem. Front.*, 2022, **9**, 1770–1776.
44 M. M. Ndiaye, S. Pillet, E. E. Bendeif, M. Marchivie, G. Chastanet, K. Boukheddaden and S. Triki, *Eur. J. Inorg. Chem.*, 2018, **2018**, 305–313.
45 E. Milin, V. Patinec, S. Triki, E. E. Bendeif, S. Pillet, M. Marchivie, G. Chastanet and K. Boukheddaden, *Inorg. Chem.*, 2016, **55**, 11652–11661.
46 M. Ahmed, K. A. Zenere, N. F. Sciortino, K. S. A. Arachchige, G. F. Turner, J. Cruddas, C. Hua, J. R. Price, J. K. Clegg, F. J. Valverde-Muñoz, J. A. Real, G. Chastanet, S. A. Moggach, C. J. Kepert, B. J. Powell and S. M. Neville, *Inorg. Chem.*, 2022, **61**, 6641–6649.
47 Y. C. Chen, Y. Meng, Y. J. Dong, X. W. Song, G. Z. Huang, C. L. Zhang, Z. P. Ni, J. Navařík, O. Malina, R. Zbořil and M. L. Tong, *Chem. Sci.*, 2020, **11**, 3281–3289.
48 R. Ketkaew, Y. Tantirungrotechai, P. Harding, G. Chastanet, P. Guionneau, M. Marchivie and D. J. Harding, *Dalton Trans.*, 2021, **50**, 1086–1096.
49 N. Phukkaphan, D. L. Cruickshank, K. S. Murray, W. Phonsri, P. Harding and D. J. Harding, *Chem. Commun.*, 2017, **53**, 9801–9804.
50 B. J. C. Vieira, J. T. Coutinho, I. C. Santos, L. C. J. Pereira, J. C. Waerenborgh and V. Da Gama, *Inorg. Chem.*, 2013, **52**, 3845–3850.
51 K. D. Murnaghan, C. Carbonera, L. Toupet, M. Griffin, M. M. Dîrtu, C. Desplanches, Y. Garcia, E. Collet, J. F. Létard and G. G. Morgan, *Chem.–Eur. J.*, 2014, **20**, 5613–5618.
52 F. F. Martins, A. Joseph, H. P. Diogo, M. E. Minas da Piedade, L. P. Ferreira, M. D. Carvalho, S. Barroso, M. J. Romão, M. J. Calhorda and P. N. Martinho, *Eur. J. Inorg. Chem.*, 2018, 2976–2983.
53 K. Miyano, T. Nishida, H. Ono, D. Hamada, T. Fujinami, N. Matsumoto and Y. Sunatsuki, *Inorg. Chim. Acta*, 2016, **439**, 49–54.
54 Z. Liu, Z. Yao and J. Tao, *Inorg. Chem.*, 2021, **60**, 10291–10301.
55 R. Kulmaczewski, E. Trzop, L. J. Kershaw Cook, E. Collet, G. Chastanet and M. A. Halcrow, *Chem. Commun.*, 2017, **53**, 13268–13271.
56 V. Russell, M. Scudder and I. Dance, *J. Chem. Soc., Dalton Trans.*, 2001, 789–799.
57 J. Cruddas and B. J. Powell, *Inorg. Chem. Front.*, 2020, **7**, 4424–4437.
58 K. Jonas, A. Jean-Paul, C. Renée, C. Epiphane, K. Olivier, J. G. Haasnoot, G. Françoise, J. Charlotte, A. Bousseksou, L. Jorge, V. François and G. V. Anne, *Chem. Mater.*, 1994, **6**, 1404–1412.
59 R. D. Shannon, *Acta Crystallogr., Sect. A: Found. Adv.*, 1976, **32**, 751–767.
60 R. Bertoni, M. Lorenc, J. Laisney, A. Tissot, A. Moréac, S. F. Matar, M. L. Boillot and E. Collet, *J. Mater. Chem. C*, 2015, **3**, 7792–7801.
61 M. Gakiya-Teruya, X. Jiang, D. Le, Ö. Üngör, A. J. Durrani, J. J. Koptur-Palenchar, J. Jiang, T. Jiang, M. W. Meisel, H. Cheng, X.-G. Zhang, X. Zhang, T. S. Rahman, A. F. Hebard and M. Shatruk, *J. Am. Chem. Soc.*, 2021, **143**, 14563–14572.
62 G. Chastanet, C. Desplanches, C. Baldé, P. Rosa, M. Marchivie and P. Guionneau, *Chem*, 2018, 1–19.
63 Y. S. Ye, X. Q. Chen, Y. De Cai, B. Fei, P. Dechambenoit, M. Rouzières, C. Mathonière, R. Clérac and X. Bao, *Angew. Chem., Int. Ed.*, 2019, **58**, 18888–18891.